AGU PUBLICATIONS

Tectonics

RESEARCH ARTICLE
10.1002/2017TC004574

Key Points:
- Two phases of intracontinental reactivation, during the Early to Middle Triassic and Late Cretaceous, are revealed in the easternmost Tianshan
- Extent of strain propagation from various Meso-Cenozoic Eurasian plate margin events is clarified
- Exhumation in response to India-Eurasia collision was insufficient to be detected by low-temperature thermochronology

Supporting Information:
- Supporting Information S1
- Data Set S1

Correspondence to:
J. Gillespie,
jack.gillespie@adelaide.edu.au

Citation:
Gillespie, J., Glorie, S., Jepson, G., Zhang, Z. Y., Xiao, W. J., Danišík, M., & Collins, A. S. (2017). Differential exhumation and crustal tilting in the easternmost Tianshan (Xinjiang, China), revealed by low-temperature thermochronology. *Tectonics*, *36*, 2142–2158. https://doi.org/10.1002/2017TC004574

Received 21 MAR 2017
Accepted 16 SEP 2017
Accepted article online 25 SEP 2017
Published online 23 OCT 2017

Differential Exhumation and Crustal Tilting in the Easternmost Tianshan (Xinjiang, China), Revealed by Low-Temperature Thermochronology

J. Gillespie[1], S. Glorie[1], G. Jepson[1], Z. Y. Zhang[2], W. J. Xiao[2,3], M. Danišík[4], and A. S. Collins[1]

[1]Centre for Tectonics, Resources, and Exploration (TRaX), School of Physical Sciences, Department of Earth Sciences, University of Adelaide, Adelaide, South Australia, Australia, [2]State Key Laboratory of Lithospheric Evolution, Institute of Geology and Geophysics, Chinese Academy of Sciences, Beijing, China, [3]Xinjiang Research Centre for Mineral Resources, Xinjiang Institute of Ecology and Geography, Chinese Academy of Sciences, Urumqi, China, [4]John de Laeter Centre, Applied Geology, TIGeR, Curtin University, Perth, Western Australia, Australia

Abstract The easternmost Tianshan forms the eastern extremity of the modern Central Asian Orogenic Belt and represents a key locality to investigate strain propagation from the Meso-Cenozoic plate margins to the Eurasian interior. The Tianshan as a whole has been reactivated multiple times throughout the Meso-Cenozoic, but the extent of these reactivation events is yet to be fully understood. This study applies apatite fission track and apatite (U-Th-Sm)/He thermochronology to the mountain ranges of the easternmost Tianshan. Our new results suggest that the area experienced two phases of rapid cooling in the Mesozoic —during the Early to Middle Triassic and the Late Cretaceous. These cooling phases are linked to tectonic events at the distant plate margins such as the Permian to Middle Triassic closure of the Paleoasian Ocean and the Late Jurassic to Early Cretaceous Mongol Okhotsk orogeny. Fault-controlled differential exhumation and block tilting are recorded in the distribution of apatite fission track ages across the region. Finally, we show through a combination of multiple thermochronometers and the integration of structural analysis that the easternmost Tianshan has experienced insufficient exhumation to constrain the timing of reactivation in response to the Cenozoic collision of India with Eurasia and instead records older, Mesozoic tectonic events.

1. Introduction

The Central Asian Orogenic Belt (CAOB) is the largest intracontinental deformation belt in the world (Windley et al., 2007; Xiao et al., 2004) and is an ideal natural laboratory for the study of intracontinental reactivation. The CAOB has experienced several phases of reactivation in response to tectonic events at the Eurasian plate margin since its amalgamation in the Paleozoic, most notably in response to the ongoing India-Eurasia collision (e.g., De Grave et al., 2007; Glorie & De Grave, 2016; Jolivet et al., 2010; Molnar & Tapponnier, 1975).

The Tianshan is currently the largest of several intracontinental mountain belts within the CAOB that formed in response to the collision of India and Eurasia, stretching more than 2,500 km through the Central Asian republics into northwestern China (Windley et al., 1990). The easternmost extent of the mountain belt is located within the Xinjiang Uyghur Autonomous Region of China, terminating just short of the Mongolian border (Figure 1). A multitude of low-temperature thermochronological studies utilizing the apatite fission track (AFT) and/or (U-Th)/He (AHe) systems have attempted to constrain the cooling history of the Tianshan, generally concluding that the onset of modern mountain building occurred at ~25–15 Ma in response to the India-Eurasia convergence (Bande et al., 2017; De Grave et al., 2013; Dumitru et al., 2001; Glorie & De Grave, 2016; Glorie et al., 2011; Hendrix et al., 1994; Käßner et al., 2016; Macaulay et al., 2014, 2013; Shen et al., 2006; Sobel, Chen, et al., 2006; Sobel & Dumitru, 1997; Wang, Li, et al., 2009). These Oligocene-Miocene ages were mainly obtained for samples taken in the vicinity of the major fault zones and associated steep topography within the Tianshan in Kyrgyzstan, Tajikistan and western Xinjiang. Away from major reactivated faults and in regions of relatively subdued topography, relict Mesozoic ages have been reported as the amount of exhumation is not sufficient to expose deeper crustal levels with Cenozoic AFT ages (De Grave et al., 2013; Glorie et al., 2011).

Previous work within the easternmost Tianshan, however, revealed young (Oligocene-Miocene) AFT ages (Wang et al., 2008), which were interpreted as recording exhumation related to progressive eastwards reactivation in response to the ongoing India-Eurasia collision. The young, regionally distributed AFT ages found

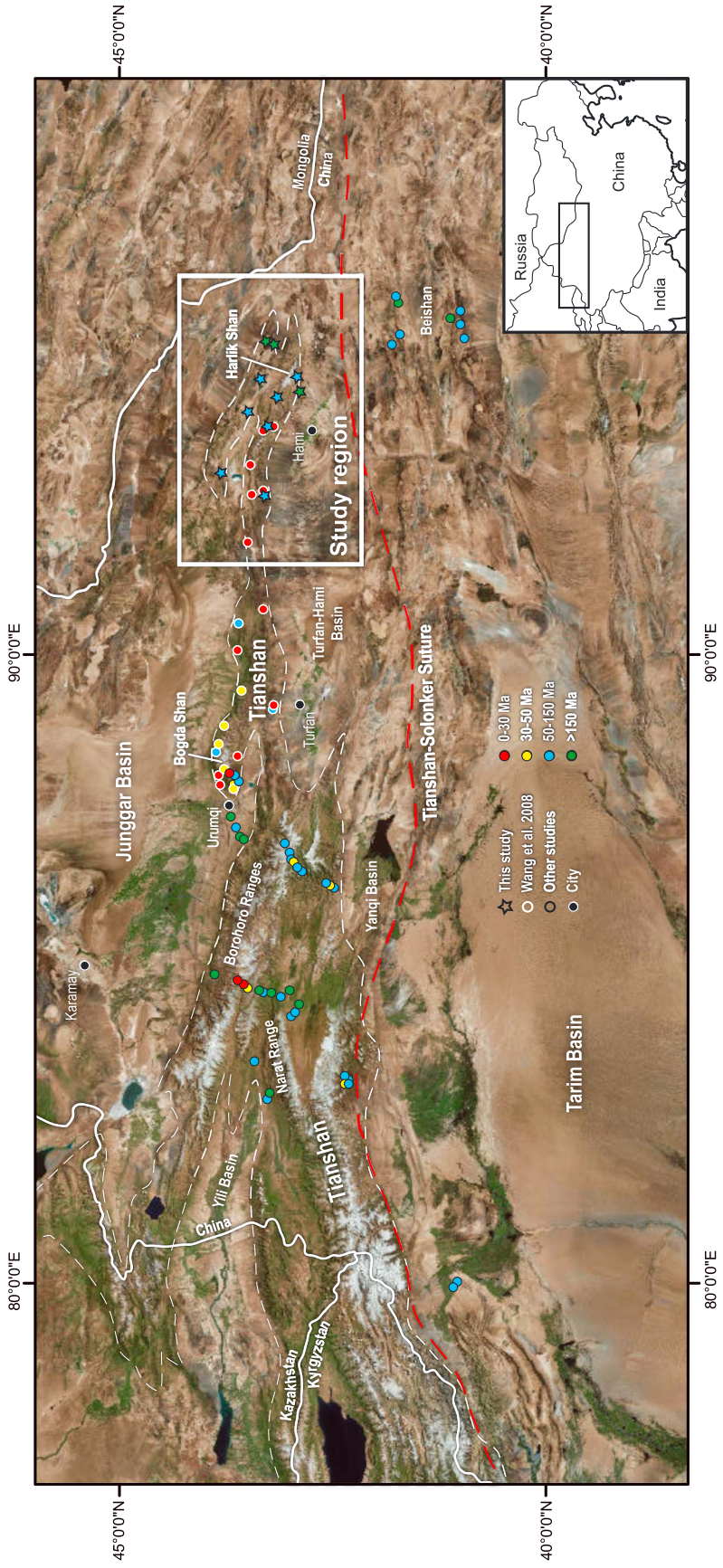

Figure 1. Satellite map of the eastern Tianshan and NW China. Published apatite fission track central ages from the Chinese Tianshan and immediate surrounds are indicated by colored dots. White dashed line indicates extent of the Tianshan. Stars are central ages from this study. Data are from Dumitru et al. (2001), Ma, Shu, and Zhu (2006), Shen et al. (2008), Wang et al. (2008), Wang, Li, et al. (2009), Zhang et al. (2009), Jolivet et al. (2010), Lü et al. (2013), Tang et al. (2015), Tian et al. (2016), and Gillespie et al. (2017).

by Wang et al. (2008) spurred this study to further investigate the thermotectonic history of the easternmost Tianshan, particularly due to the apparent value of those young ages in providing insight into the nature and timing of late Cenozoic reactivation in the eastern Tianshan.

2. Background

2.1. Structural Architecture

The easternmost Tianshan comprises three ranges that strike roughly NW-SE. The Balikun Shan and Harlik Shan (also known as Barkol Tagh and Karlik Tagh) are located to the south of the slightly lower Dahei Shan (Figure 2). The ranges of the easternmost Tianshan are bound by doubly vergent outward directed thrusts, forming asymmetric flower structures that control the exhumation of the study area (Cunningham et al., 2003). Asymmetric drainage patterns and slope profiles in the Balikun and Harlik Ranges suggest that the northern flanks have experienced more extensive uplift and exhumation. The apparent lack of major faults within the core of the ranges, in conjunction with topographic analysis, led Cunningham et al. (2003) to conclude that both ranges were largely uplifted as single contiguous blocks undergoing southward tilting. Cunningham et al. (2003) furthermore noted the presence of a Late Cretaceous to early Cenozoic planation surface preserved in many parts of the study area, prominently on the southern slopes of Harlik Shan and on more spatially limited areas of Balikun Shan. Planation surfaces of this age are also preserved in western Mongolia and in other parts of the Chinese Tianshan (Devyatkin, 1974; Heilbronn et al., 2015). This planation surface provides important constraints on the interpretation of thermochronological data from the study area.

The major bounding faults to the north and south of the ranges experienced ductile deformation from the Late Permian to Early Triassic and were subsequently reactivated as brittle faults (Cunningham et al., 2003). These faults thrust older rock over Quaternary sediment, offset alluvial fans, and have a historical record of seismicity that attests to their ongoing activity (Cunningham, 2013). Brittle reactivation of inherited structural elements is also common elsewhere in the Tianshan (e.g., Glorie et al., 2011; Macaulay et al., 2014).

2.2. Basement History

The easternmost Tianshan is tectonically part of the Paleozoic Harlik Arc, which constitutes the northern half of the Harlik-Dananhu arc system. The Harlik Arc was formed during the southwards subduction of the Kelaimeili Ocean, prior to its closure in the Carboniferous (Xiao et al., 2004). The terminal suture resulting from this closure defines the northern margin of the arc system. The Harlik-Dananhu arc system is correlated to the west with the Chinese northern Tianshan (Windley et al., 1990).

The Harlik Arc consists of rocks that range from Ordovician to Permian in age. Devonian-Carboniferous arc-related volcanic rocks with a broad range of compositions are abundant, as are Carboniferous flysch sequences (Xiao et al., 2004). The region also features numerous Devonian-Carboniferous igneous intrusions and Late Carboniferous to Early Permian postcollisional granites (Figure 2; Ma et al., 2015).

3. Samples and Methods

3.1. Sample Locations

Samples were collected as widely as possible from intrusive igneous bodies throughout the study area. Where practical, structures identified in Cunningham et al. (2003) were targeted for sampling. Eighteen samples were taken from Devonian-Permian granitoids within all three of the ranges of the easternmost Tianshan (Figure 2). Ten samples span the entire length of the southern slopes and eastern extent of Dahei Shan. Five samples were taken from around the margins of Harlik Shan, and three samples were taken from Balikun Shan. Sample descriptions, including geographical locations, can be found in Table 1.

3.2. Apatite Fission Track Analysis

The apatite fission track dating method integrates information about the cooling history of apatite crystals in the upper crust in the temperature range of ~60°C to ~120°C, known as the apatite partial annealing zone (APAZ) (Gleadow et al., 1986). The exact temperature range of the APAZ depends on the cooling rate and the chemistry of the individual apatite grains (Ketcham et al., 1999). Typically, chlorine content (Cl wt %) is considered to be the dominant annealing control in apatite (Green et al., 1986). The *c* axis etch pit

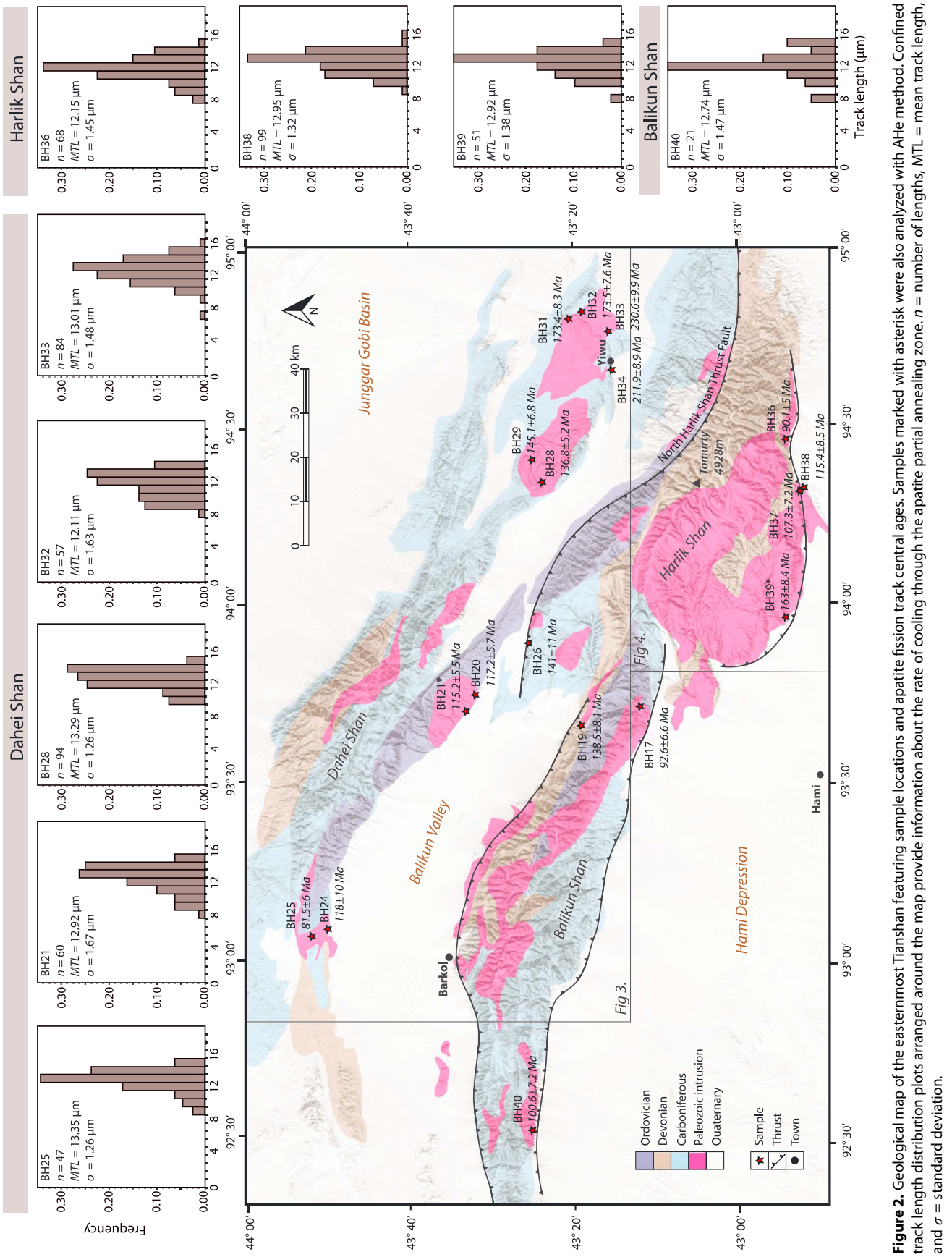

Figure 2. Geological map of the easternmost Tianshan featuring sample locations and apatite fission track central ages. Samples marked with asterisk were also analyzed with AHe method. Confined track length distribution plots arranged around the map provide information about the rate of cooling through the apatite partial annealing zone. *n* = number of lengths, MTL = mean track length, and σ = standard deviation.

Table 1
Sample Locations and Lithologies

Sample	IGSN	Latitude (WGS84)	Longitude (WGS84)	Altitude (m a.s.l.)	Locality	Lithology
Balikun:						
BH17	IEJAG000H	N43°12.042	E93°42.618	1851	Southern Balikun mountain pass	Granite
BH19	IEJAG000I	N43°19.467	E93°40.083	2343	Northern Balikun mountain pass	Mylonite/amphibolite
BH40	IEJAG000Y	N43°24.656	E92°30.608	2073	Southern margin Balikun Shan	Granite
Dahei:						
BH20	IEJAG000J	N43°31.324	E93°44.982	2088	North of pass, central Dahei Shan	Granite
BH21	IEJAG000K	N43°32.284	E93°42.609	2096	North of pass, central Dahei Shan	Granite
BH24	IEJAG000L	N43°50.119	E93°04.907	1786	Northwestern Dahei Shan	Granodiorite
BH25	IEJAG000M	N43°51.793	E93°03.867	1794	Northwestern Dahei Shan	Granodiorite
BH28	IEJAG000O	N43°23.803	E94°20.759	2353	Southeast Dahei Shan	Granite
BH29	IEJAG000P	N43°24.843	E94°23.741	1839	Southeast Dahei Shan	Granite
BH31	IEJAG000Q	N43°19.482	E94°49.066	1423	Southeast Dahei Shan	Granodiorite
BH32	IEJAG000R	N43°18.261	E94°49.616	1608	Southeast Dahei Shan	Granite
BH33	IEJAG000S	N43°15.088	E94°46.290	1677	Southeast Dahei Shan	Granite
BH34	IEJAG000T	N43°14.963	E94°40.458	1741	Southeast Dahei Shan	Dolerite
Harlik:						
BH26	IEJAG000N	N43°25.329	E93°54.175	2317	Northern margin Harlik Shan	Diorite
BH36	IEJAG000U	N42°53.790	E94°28.342	2270	Southern margin Harlik Shan	Deformed granodiorite
BH37	IEJAG000V	N42°52.302	E94°20.645	1740	Southern margin Harlik Shan	Diorite
BH38	IEJAG000W	N42°51.740	E94°21.019	1656	Southern margin Harlik Shan	Deformed granite-gneiss
BH39	IEJAG000X	N42°53.787	E93°56.970	1090	Southern margin Harlik Shan	Granite

Note. IGSN = International geosample number. m a.s.l. (meters above sea level).

diameter (D_{par}) is often used as a proxy for this parameter (Ketcham et al., 1999). Other unquantified parameters may act as controls on the annealing of fission tracks, as Cl wt % and D_{par} often do not adequately explain all the variability in individual AFT grain ages (Barbarand et al., 2003). Some authors have suggested that the concentration of uranium may (by various mechanisms) influence the rate of annealing in apatite (Carpena et al., 1988; Hendriks & Redfield, 2005), although this is not widely accepted.

For this study, spontaneous tracks were etched in 5.0 *M* HNO_3 for 20 ± 1 s at 20.0 ± 0.5°C (Donelick et al., 1999). Fission track densities and confined track lengths were measured using the FastTracks software after image capture on a Zeiss AXIO Imager M2m Autoscan system at the University of Adelaide (Gleadow et al., 2009). ^{238}U concentrations in apatite grains were measured directly using the NewWave 213 ablation system coupled to the Agilent 7500 mass spectrometer. Ages and uncertainties were calculated as described in Hasebe et al. (2004) using session-specific zeta-calibration calculated against repeated measurements of the Durango apatite age standard (McDowell et al., 2005). Further details can be found in Glorie et al. (2017). Radial plots (Galbraith, 1990) of single-grain ages were constructed using the RadialPlotter program (Vermeesch, 2009).

3.3. Apatite (U-Th-Sm)/He Analysis

The apatite (U-Th-Sm)/He (AHe) dating method relies on accumulation and temperature sensitive diffusion of radiogenic He in apatite crystals (Ehlers & Farley, 2003). Partial retention of He occurs between ~40°C and ~85°C (depending on the crystal size and cooling rate), allowing for the refinement of the low-temperature thermal history reconstructed from the AFT data (Wolf et al., 1998). Samples for (U-Th-Sm)/He analysis were selected based on the AFT results obtained for the sample, the structural position of the sample within the study area, and the sample quality (Farley, 2002). AHe analysis was performed on two samples (BH21 and BH39) at the John de Laeter Centre at Curtin University following procedure outlined in Evans et al. (2005), Danišík, Kuhlemann, et al. (2012), and Danišík, Štěpančíková, et al. (2012). Apatite crystals were hand-picked following the recommendation of Farley (2002). For each sample, five apatite crystals of similar size and shape were selected, then photographed, measured for physical dimensions and loaded in platinum tubes. ^{4}He was extracted from single-grain aliquots by heating to ~960°C using a diode laser under ultrahigh vacuum and measured by isotope dilution on a Pfeiffer Prisma QMS-200 mass spectrometer. Following He measurements, the apatites were spiked with ^{235}U and ^{230}Th and dissolved in nitric acid. The solutions were analyzed by isotope dilution for U and Th, and by external calibration for Sm on an Agilent 7500 ICP-MS. The total analytical

Table 2
Apatite Fission Track Data

Sample	n	ρ_s ($\times 10^5$ cm^{-2})	N_s	^{238}U (ppm)	D_{par} (μm)	t (Ma ± 1σ)	MTL (μm)	SD (μm)	N_{length}
Balikun:									
BH17	37	5.86	409	14.26	1.3	**92.6 ± 6.6**	-	-	-
BH19	40	3.84	447	6.14	1.8	**138.5 ± 8.1**	-	-	-
BH40	13	25.17	491	59.15	1.7	**100.6 ± 7.2**	12.74	1.47	21
Dahei:									
BH20	37	6.40	1075	11.66	1.4	**117.2 ± 5.7**	-	-	-
BH21	44	4.64	1329	8.56	1.4	**115.2 ± 5.5**	12.92	1.67	60
BH24	14	9.01	141	15.41	1.5	**118.0 ± 10.0**	-	-	-
BH25	15	48.13	1223	127.42	2.1	**81.5 ± 6.0**	13.35	1.26	47
BH28	40	18.25	1595	28.72	2.0	**136.8 ± 5.2**	13.29	1.26	94
BH29	36	11.22	1203	16.08	1.8	**145.1 ± 6.8**	-	-	-
BH31	35	18.86	1471	21.92	1.7	**173.4 ± 8.3**	-	-	-
BH32	37	8.29	1021	11.08	1.1	**173.5 ± 7.6**	12.11	1.63	57
BH33	36	13.73	1242	14.01	1.8	**230.6 ± 9.9**	13.01	1.48	84
BH34	39	5.17	795	4.86	2.0	**211.9 ± 8.9**	-	-	-
Harlik:									
BH26	31	2.66	171	4.03	2.1	**141.0 ± 11.0**	-	-	-
BH36	36	7.89	1035	22.92	1.8	**90.1 ± 5.0**	12.15	1.45	68
BH37	24	7.90	377	15.58	1.7	**107.3 ± 7.2**	-	-	-
BH38	24	12.05	701	23.34	1.4	**115.4 ± 8.5**	12.95	1.32	99
BH39	34	10.58	1348	13.05	1.4	**163.0 ± 8.4**	12.92	1.38	51

Note: n is the number of analyzed grains. ρ_s is the density of spontaneous tracks. N_s is the total number of counted spontaneous tracks. ^{238}U is the average concentration of ^{238}U. D_{par} is the etch pit length parallel to the c axis. T is the apatite fission track central age produced by RadialPlotter (Vermeesch, 2009). MTL is the mean length of confined tracks. SD is the standard deviation of the measured lengths. N_{length} is the number of measured confined tracks. Zeta value of $1.96 \pm 0.04 \times 10^{-3}$ calculated following Vermeesch (2017). Individual grain data are available in Table S1.

uncertainty (TAU) was calculated as a square root of sum of squares of uncertainty on He and weighted uncertainties on U, Th, and Sm measurements. The raw apatite (U-Th)/He ages were corrected for alpha ejection (Ft correction) after Farley et al. (1996), whereby a homogenous distribution of U, Th, and Sm was assumed for the crystals. Replicate analyses of Durango apatite (n = 6) measured over the period of this study as internal standard yielded mean (U-Th-Sm)/He age of 31.8 ± 1.5 Ma, which is good agreement with the reference Durango (U-Th-Sm)/He age of 31.02 ± 1.01 Ma (Farley, 2002; McDowell et al., 2005).

3.4. Thermal History Modeling

Fission track age, confined length, and apatite (U-Th-Sm)/He data were modeled using QTQt version 5.6.0 to explore the likely low-temperature cooling histories of the study area (Gallagher, 2012). QTQt uses a "Bayesian transdimensional Markov Chain Monte Carlo (MCMC)" approach to model the thermal history of a sample or set of samples. A thorough explanation of the theory and mathematics is provided in Gallagher (2012). In general, an initial unconstrained run is performed to explore the statistical space, followed by adjustments to the search parameters or the addition of geological constraints where necessary. This approach follows the Bayesian philosophy of the software, which seeks to minimize the complexity of the model by statistical means. Many iterations ($>>$ 10,000) are run to generate a range of models that create a probability distribution, from which individual models can be selected, including the maximum likelihood and "expected" (weighted mean) paths. The range of the general prior was set as t = AFT central age ±AFT central age, temperature = 70 ± 70°C. Acceptance rates for models were between 0.2 and 0.6 and birth-death ratio was ~1. Spherical geometry and the radiation damage model of Gautheron et al. (2009) were used for modeling AHe data. The annealing model from Ketcham et al. (2007) was used for fission track data with D_{par} as kinetic parameter.

4. Results

4.1. Apatite Fission Track

Eighteen samples were analyzed using the AFT method, producing exclusively Mesozoic central ages. Central ages were dominantly Cretaceous, with the exception of several samples in the east of the study area that preserved Jurassic or Triassic ages (Table 2).

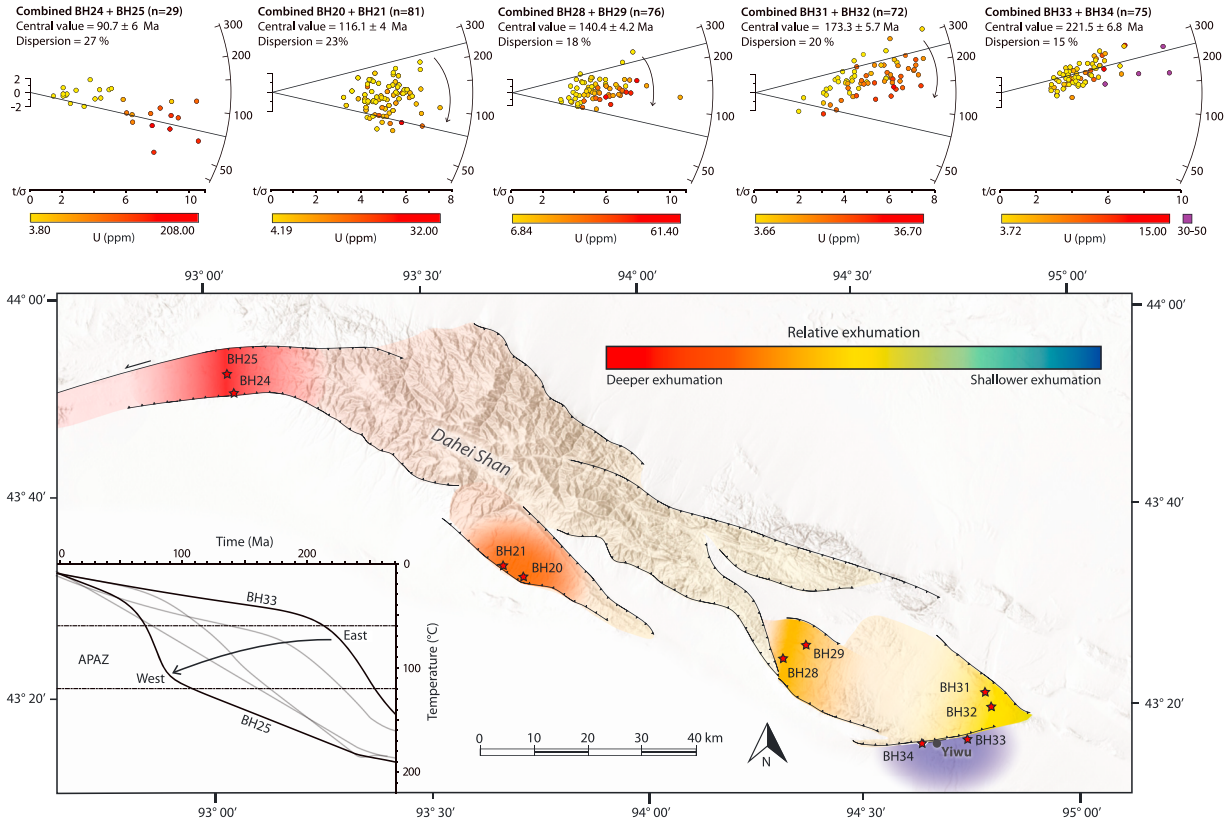

Figure 3. Hillshade DEM of Dahei Shan with overlay depicting the amount of relative exhumation. Radial plots of single grain ages at top of figure display "open jaw" pattern linked to partial reset between thermal events. Modeled timing of enhanced cooling shown by lines on radial plots, with arrows indicating possible reset. Inset simplified thermal history models show weighted mean cooling paths for individual samples. See Figure 5 for full models.

4.1.1. Dahei Shan

Traversing from east to west along Dahei Shan, central ages become progressively younger, particularly as major faults are crossed, and the obtained AFT results are therefore discussed accordingly (Figure 3). The 10 samples that were analyzed for the Dahei Shan can be grouped into five pairs that have similar central ages. The easternmost block of the Dahei Shan is an eastwards closing wedge controlled by a pair of outward directed thrust faults (Cunningham et al., 2003). Four samples were taken in the vicinity of those thrust faults. The two samples closest to the town of Yiwu (Figure 3) lie to the south of an EW trending fault that demarcates the ridge front to the north of the town. This area is the southeasternmost extent of the Dahei Shan range. The central ages of these samples (BH33 and BH34) are the oldest for the entire area at 230.6 ± 9.9 Ma and 211.9 ± 8.9 Ma, respectively (Table 2 and Figures S1 and S2 in the supporting information). Sample BH33 has a mean track length (MTL) of 13.01 μm with a standard deviation of 1.48 μm (Figure 2 and Table 2).

Just north of BH34 and BH33, over the thrust fault, identical central ages of 173.4 ± 8.3 Ma and 173.5 ± 7.6 Ma were obtained for samples BH31 and BH32, respectively (Figure 3). Sample BH32 has a MTL of 12.11 μm and a standard deviation of 1.63 μm. Further to the west, within the same major structural block of the Dahei Shan, BH28 and BH29 produce ages of 136.8 ± 5.2 Ma and 145.1 ± 6.8 Ma, respectively. A significant elevation difference (BH28 ~ 500 m higher) potentially contributes to the age disparity (Table 1). However, much like the easternmost samples, overlapping uncertainties demonstrate the strong similarity between these two samples. BH28 has a MTL of 13.29 μm and a standard deviation of 1.26 μm. On the southern margin of Dahei Shan, near the center of the range, BH20 and BH21 yield identical central ages of 117.2 ± 5.7 Ma and 115.2 ± 5.5 Ma. BH21 has a MTL of 12.92 μm and a standard deviation of 1.67 μm. The westernmost and youngest sample from Dahei Shan is BH25, with a central age of 81.5 ± 6 Ma. BH25 has a MTL of 13.35 ± 1.26 μm, the longest of any sample in the study region. It is accompanied by BH24, with an older central age of 118 ± 10 Ma (Table 2).

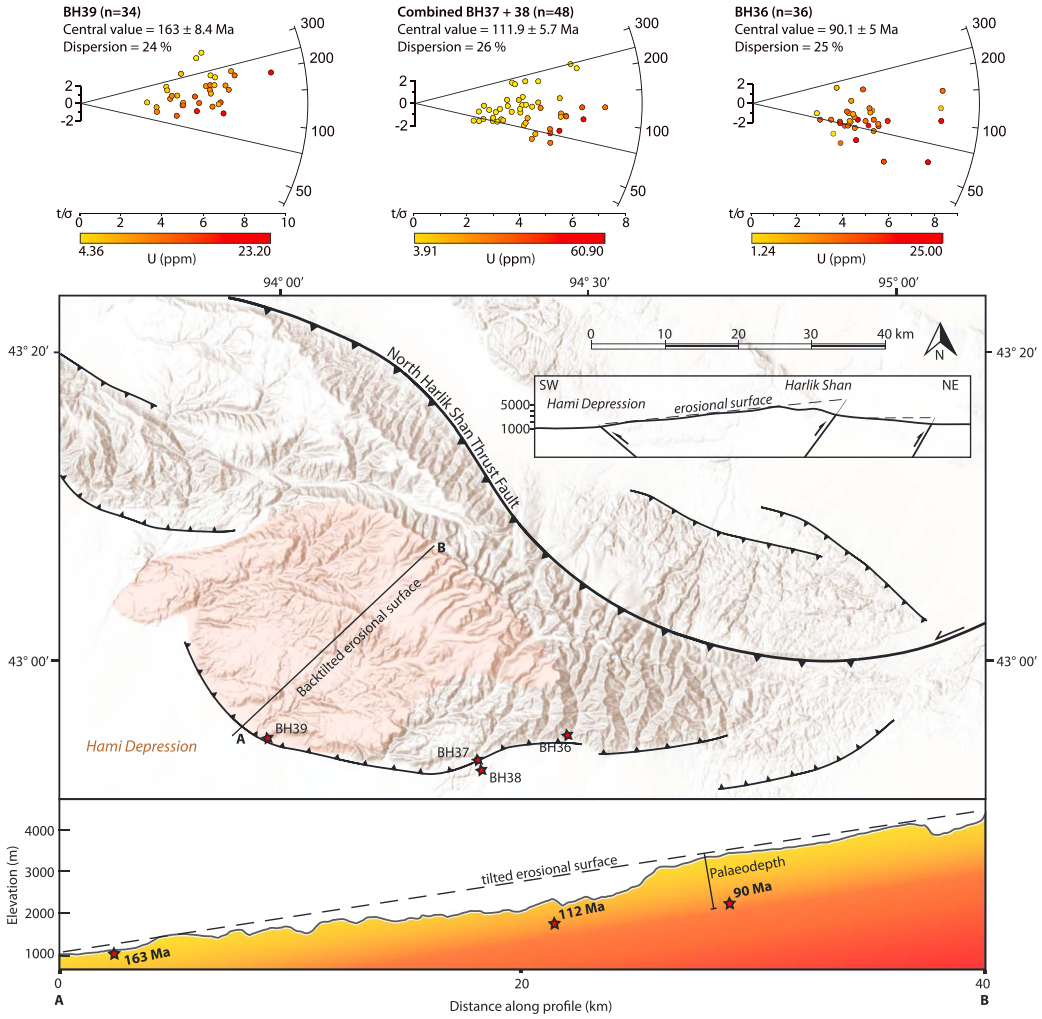

Figure 4. Detail of Harlik Shan illustrating the tilted peneplain identified by Cunningham et al. (2003) that composes the southern flank of the mountain. Elevation profile shows planation surface with schematic preserved thermal structure based on AFT ages, represented by the color gradient. AFT sample locations are projected onto profile based on elevation and location within the tilted peneplain. Modeled timing of enhanced cooling shown by lines on radial plots.

4.1.2. Harlik Shan

Five samples were taken from Harlik Shan, one on the northern margin, and four on the southern margin. The northern flank of Harlik Shan (BH26) recorded a central age of 141 ± 11 Ma. The four samples from the southern margin of the mountain are arrayed west-east, becoming younger to the east. The westernmost sample (BH39) has the oldest central age of 163 ± 8.4 Ma and was taken at the lowest elevation of these samples, near to the planation surface (Figure 4). It has a MTL of 12.92 μm and a standard deviation of 1.38 μm. BH37 and BH38 have similar central ages of 107.3 ± 7.2 Ma and 115.4 ± 8.5 Ma, respectively, with sample locations around 1 km apart and no intervening major structures. BH38 has a MTL of 12.95 μm and a standard deviation of 1.32 μm. Taken from within a deeply incised valley to the east, BH36 has a central age of 90.1 ± 5 Ma and a MTL of 12.15 ± 1.45 μm (Table 2).

4.1.3. Balikun Shan

Three samples were taken from Balikun Shan (Figure 2). The samples taken from the southern flank of the range produced central ages of 100.6 ± 7.2 Ma in the west (BH40) and 92.6 ± 6.6 Ma in the east (BH17). These two samples lie in a similar structural position near to the southern bounding fault of the range. On the northern flank, BH19 recorded an older central age of 138.5 ± 8.1 Ma, similar to the central age of BH26 from the northern flank of Harlik Shan (Figures S1 and S2). BH19 was also taken from a higher altitude (2343 m) than BH17 (1851 m) or BH40 (2073 m, Table 1).

Table 3
Apatite (U-Th-Sm)/He Data

Sample	Th (ng)	± (%)	U (ng)	± (%)	Sm (ng)	± (%)	He (ncc)	± (%)	TAU (%)	Th/U	Unc. Age (ma)	±1σ (ma)	Ft	Cor. Age (ma)	±1σ (ma)
21:															
a	0.004	5.4	0.007	5.5	0.018	0.4	0.331	3.1	5.7	0.56	349.3	19.9	0.62	**559.8**	**42.4**
c	0.011	4.0	0.017	4.0	0.028	0.3	0.468	2.8	4.4	0.62	190.7	8.5	0.66	**287.2**	**19.2**
b	0.006	5.4	0.024	5.6	0.028	0.7	0.189	3.6	6.3	0.25	60.5	3.8	0.59	**102.7**	**8.3**
d	0.092	3.8	0.063	4.0	0.130	0.2	1.471	2.9	4.2	1.45	140.1	5.9	0.77	**182.4**	**11.9**
e	0.030	5.3	0.021	5.5	0.041	0.3	0.291	3.4	5.4	1.43	83.7	4.5	0.59	**140.9**	**10.4**
39:															
a	0.219	5.3	0.135	5.5	0.023	0.4	0.671	1.9	4.6	1.62	29.6	1.4	0.64	**46.0**	**3.1**
b	0.039	3.8	0.009	4.0	0.005	0.4	0.578	2.7	3.8	4.05	251.0	9.6	0.62	**404.3**	**25.5**
c	0.211	5.3	0.043	5.5	0.021	0.3	1.206	2.4	4.5	4.85	105.9	4.8	0.64	**165.2**	**11.1**
d	0.090	3.8	0.023	4.0	0.012	0.5	0.428	1.9	3.3	3.94	79.6	2.7	0.60	**132.3**	**8.0**
e	0.063	5.4	0.028	5.5	0.007	0.6	0.264	2.0	4.5	2.27	50.9	2.3	0.58	**88.1**	**5.9**

Note. Th is ^{232}Th, U is ^{238}U, and Sm is ^{147}Sm in ng (nanogram). He is ^{4}He in ncc (nanocubic centimeter). TAU is the total analytical uncertainty. Unc. Age is the uncorrected he age. Ft is the alpha recoil correction factor after Farley et al. (1996). Cor. Age is the corrected He age.

4.2. Apatite (U-Th-Sm)/He

Apatite (U-Th-Sm)/He analysis was carried out on five grains from both sample BH21 (Dahei Shan) and BH39 (Harlik Shan). In both cases, highly dispersed individual grain ages were produced, ranging from 46.0 ± 3.1 Ma to 559.8 ± 42.4 Ma (Table 3). After discounting the three grains with AHe ages older than zircon U-Pb ages (288 ± 3 Ma, Daliugou Pluton, BH21; 298 ± 2 Ma, Badashi Pluton, BH39) for the sampled intrusions (Wang, Gu, et al., 2009; Yuan et al., 2010), the remaining grains (mostly Jurassic-Cretaceous in age) were incorporated individually into the relevant QTQt model (Gallagher, 2012) using the radiation damage model of Gautheron et al. (2009).

4.3. Thermal History Modeling

Thermal history modeling was conducted for all eight samples that yielded sufficient ($> \approx 50$) confined tracks. Due to poor sample quality (e.g., small grain size, low grain yield, and low track density), many samples contained insufficient confined tracks to build an adequate population for modeling.

4.3.1. Dahei Shan

Five samples from Dahei Shan were suitable for modeling. Models were run without constraints, other than a start point based on zircon U-Pb ages of 300–285 Ma for the sampled intrusions (Ma et al., 2015). The zircon U-Pb ages were used to impose initial high temperature boxes from 350 to 250 Ma at 200 ± 20°C, chosen to allow maximum freedom for the model and to allow the data to be fully explored by the software.

The thermal history model for BH33 suggests a relatively rapid transit through the APAZ during the Triassic, entering at ~250 Ma and cooling below 60°C at ~220 Ma (Figure 5).

Samples BH32, BH28 and BH21 produced models that predict slow cooling through the APAZ during the late Triassic to Late Cretaceous. The timing of modeled cooling decreases from east to west, from BH32 at ~230–140 Ma, to BH28 at ~175–115 Ma, and BH21 at ~165–80 Ma. The model obtained for sample BH25 shows a phase of enhanced cooling through the APAZ at ~80 Ma.

4.3.2. Harlik Shan

Three samples from Harlik Shan were suitable for modeling (Figures 5 and S3). The thermal history model for Harlik Shan was constrained by a number of geological observations that by necessity introduced significant complexity to the model. Samples BH36 and BH39 from Harlik Shan belong to a monolithic block that was uplifted and tilted without the presence of intervening faults (Figure 4; Cunningham et al., 2003). The low-temperature constraint is provided by sample BH39 that was taken in proximity to the preserved planation surface that constitutes the southern flank of Harlik Shan. The proximity of BH39 to the planation surface implies that this sample must have cooled to near-surface temperatures by the time the planation surface was formed during the Late Cretaceous to early Paleogene.

As this surface was uplifted and tilted as a single block (Cunningham et al., 2003), we can estimate the pretilting vertical depth of samples taken from within the incised valleys of the uplifted section of this

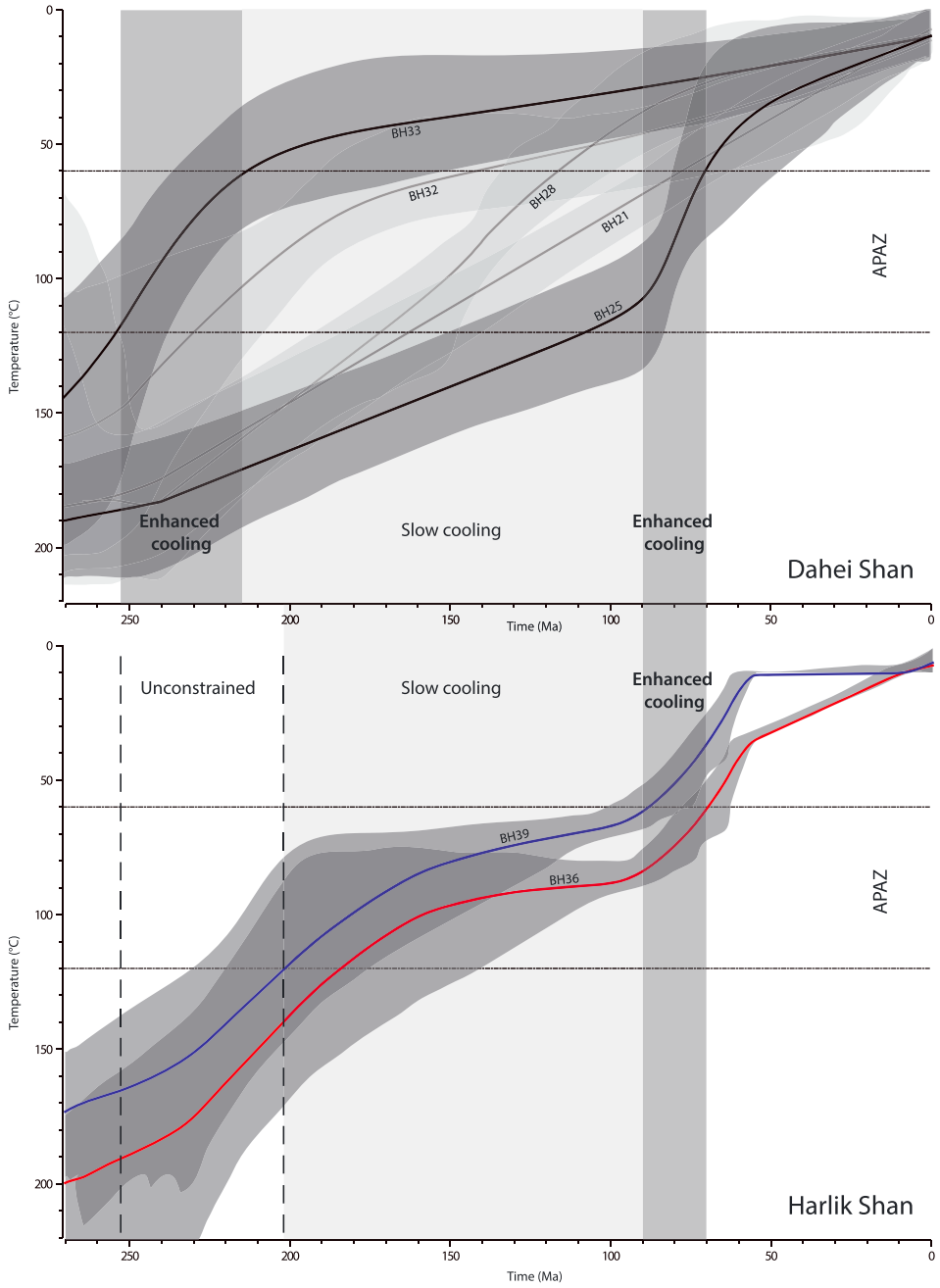

Figure 5. Thermal history models generated in QTQt (Gallagher, 2012). All models are based on AFT data, with the additional use of AHe data for BH21 and BH39. For all modeled samples the "expected" models with 95% credible intervals are displayed. The expected model is effectively the weighted mean of all the sampled thermal histories.

block with respect to the planation surface. The sample locations from the southern margin of Harlik Shan were projected onto a cross section through the peneplain defined in Cunningham et al. (2003) (Figure 4), and the relative position of the samples to the surface was calculated by creating a grid of elevation profiles across the southern flank of the mountain to identify the elevation and slope of the peneplain. The resulting age-paleodepth pattern along the cross section reveals the low-temperature thermal structure of the crust prior to tilting. Knowing the extent of this vertical separation allows us to combine samples to form a pretilting "vertical profile" and model their thermal histories together (Figure 4).

High-temperature constraints on possible thermal histories (350–250 Ma at 200 ± 20°C) were based on zircon U-Pb crystallization ages of ~300–285 Ma age for the sampled intrusions on Harlik Shan (Ma et al., 2015).

The paleodepth profile thermal history model of Harlik Shan reveals two main pulses of cooling. Initial slow cooling into the APAZ was modeled to take place at ~200–160 Ma, which brought BH36 and BH39 (red and blue lines in Figure 5, respectively) to middle and upper APAZ temperatures, according to their relative paleodepths. A subsequent period of relative quiescence kept the samples at APAZ temperatures until ~100 Ma, followed by a second phase of cooling at ~80 Ma. This Late Cretaceous cooling event brought the shallowest sample (BH39) to the surface and is similar in timing and rate to that modeled for BH25. The model predicts a late Cenozoic pulse of cooling that tilted the deeper samples to their present outcrop position; however, the actual timing of tilting cannot be obtained from our data as it is outside the validity zone of the model (below ~60°C). The model is similarly not meaningful prior to ~200 Ma as the samples are below the APAZ until this time. Modeling samples BH36 and BH39 as a pseudovertical profile provides a much more consistent and reasonable thermal history distribution when compared to modeling them separately.

Sample BH38 was modeled separately to BH36 and BH39 as there is an intervening fault. The model produced for BH38 was constrained only by a Carboniferous-Permian high-temperature box based on published zircon U-Pb ages (Ma et al., 2015) and predicted monotonic cooling from emplacement to surface temperatures (Figure S3).

5. Discussion

5.1. Thermotectonic History of the Easternmost Tianshan

5.1.1. Thermal History

Understanding the regional structure of the easternmost Tianshan is the key to interpreting its thermal history. According to structural analysis in Cunningham et al. (2003), the modern fault-bound ranges of the easternmost Tianshan were uplifted as large contiguous blocks. By applying this concept and attempting to define fault blocks according to previous work and major mapped faults, patterns in the AFT data can be deciphered and reveal a picture of the thermal history of the region.

In the northern range of the easternmost Tianshan (Dahei Shan), AFT age patterns appear to show differential fault-block exhumation, resulting in different exposure levels of the crust (and their preserved thermal structure) with respect to the relative degree of exhumation. Although the whole area probably experienced regional, widespread exhumation during the Triassic as a result of the Paleoasian Ocean closure (Xiao et al., 2009), only the area outside the fault bound range (represented by BH33/34) preserves a Triassic signal. The preservation of this age implies that the area outside the major bounding faults was not reactivated during subsequent periods of exhumation (Figure 3). North across a bounding thrust fault from BH33/34 (Figure 3), the easternmost block of the Dahei Shan records quite different central ages to those outside the ranges. In contrast to rapid cooling during the Triassic, this block records an AFT signal that suggests a more complex Mesozoic cooling history. Samples within the ranges record progressively younger ages and longer MTLs farther west along the range, with this trend culminating in sample BH25 that yields the youngest AFT age and longest MTL of the entire range (Figures 2 and 3). All of the samples from within the ranges with the exception of those in the far west (BH24/25) record relatively slow cooling during the Jurassic and Cretaceous, with extended periods of residence in the APAZ. The thermal history model based on AFT data from sample BH25, meanwhile, predicts enhanced rates of cooling at ~80 Ma.

All of the samples from Dahei Shan appear to have experienced some degree of partial reset except for BH25, which was cooled relatively rapidly through the APAZ according to thermal history modeling. Radial plots of data from the Dahei Shan samples show a transition from Early Jurassic to Late Cretaceous ages from east to west, with most samples exhibiting mixed ages reflected in moderate to high levels of dispersion (Figure 3). The mixed samples show to some extent an "open jaw" pattern (O'Sullivan & Parrish, 1995) in the radial plots (Figure 3), the spread of individual grain ages visually demonstrating the progressive amount of reset each sample has experienced depending on their depth/period of residence in the APAZ (O'Sullivan & Parrish, 1995). In many samples there is also an apparent correlation (of varying strength) between the age of a grain and its uranium concentration (Figure 3) that may suggest the uranium concentration has some influence on the annealing characteristics of the apatites (e.g., Carpena et al., 1988; Hendriks & Redfield, 2005). Although

some work has attempted to address this issue through annealing experiments (e.g., Carpena & Lacout, 2010), further experiments are clearly needed to properly explore the association. Conversely, there does not appear to be a correlation between D_{par} and age in any of the samples (Figure S1). The mostly Jurassic-Cretaceous single grain AHe ages from BH21 and BH39 are also highly dispersed. Although the causes of single grain AHe age dispersion are highly complex and remain a topic of much debate (e.g., Brown et al., 2013; Farley, 2002; Fitzgerald et al., 2006), it has been suggested that slow cooling rates may result in highly variable single grain ages (Fitzgerald et al., 2006), as seen in our results. This concept may help to explain the dispersion of our AHe ages and would be consistent with our thermal models, which suggest both BH21 and BH39 experienced extended slow cooling through much of the Jurassic and Cretaceous.

Differences in the central ages preserved at the surface today are probably due to differential exhumation of the rock that preserves this Mesozoic signal. Younger ages in the west of Dahei Shan would then imply deeper exhumation than that experienced in the east. This is consistent with the observation that on the scale of the Tianshan, there is a greater accommodation of strain in the west than in the east, related to the collision of the northwestern extent of the Indian plate with Eurasia, and the associated clockwise rotation of the Tarim block (e.g., Avouac et al., 1993).

The backtilted planation surface that constitutes the southern flank of Harlik Shan provides important insight into the thermal structure of the crust prior to the modern uplift of the ranges. The age-paleodepth pattern across the block reveals the low-temperature thermal structure of the crust prior to tilting. Samples taken from progressively more deeply incised valleys record younger AFT ages, reflecting their deeper position below the ancient surface. The model for Harlik Shan (Figure 5) shows that the samples were brought up into the APAZ at some point in the Triassic-Jurassic, remaining there until the top sample was exhumed to near surface by the Late Cretaceous, in time for the development of the Late Cretaceous-early Paleogene planation surface (Cunningham et al., 2003). This ~80 Ma cooling phase is similar in timing and rate to the major phase of cooling modeled for BH25.

5.1.2. Tectonic Context

The results presented in this paper record the Meso-Cenozoic thermal history of the study region. As the tectonic amalgamation of the Harlik-Dananhu Arc was complete by the Late Carboniferous (Xiao et al., 2004), the Meso-Cenozoic events that induced cooling of the easternmost Tianshan must have occurred in an intracontinental setting. Triassic cooling is the oldest signal recorded in the study area, preserved solely on the fringes of the easternmost Tianshan outside the main fault-bound ranges. Thermal modeling of sample BH33 suggests cooling at ~250–230 Ma (Figure 5), coeval with ^{40}Ar-^{39}Ar ages attributed to ductile thrusting along the major mylonitic bounding faults of Balikun and Harlik Shan (Cunningham et al., 2003). Indeed, widespread activity along major shear zones throughout Central Asia occurred during the Permian to Early Triassic, related to large-scale block rotation and reorganization (e.g., Allen et al., 2006; Laurent-Charvet et al., 2003). This may play a role in the cooling we see recorded in our thermochronological data. Separation of the Junggar and Turfan-Hami basins at this time (Hendrix, 2000) lends further credence to the idea that Early Triassic cooling corresponds to the generation of topography in the Paleo-Tianshan. It is also possible, due to the proximity of the Tianshan-Solonker (Paleoasian) suture to the south of the study area (Figure 1; Xiao et al., 2013), that the closure of the Paleoasian Ocean was the driver of the thermotectonic activity we see recorded at this time. The timing of the closure of the Paleoasian Ocean remains a controversial question. Some authors argue that the final closure of the Paleoasian Ocean and the collision of the Tarim Craton with the southern Siberian active margin occurred during the Late Permian to Early Triassic (Lehmann et al., 2010; Xiao et al., 2009). Alternate models suggest that final amalgamation occurred significantly earlier, during the Carboniferous or Early Permian (Biske & Seltmann, 2010; Charvet et al., 2011).

The cause of Late Cretaceous reactivation throughout Central Asia is not clear. In the western Tianshan, Cretaceous ages are sometimes attributed to the accretion of the Kohistan-Dras arc in modern Afghanistan (Hendrix et al., 1992). While this may be a plausible explanation for reactivation in the western Tianshan (e.g., De Grave et al., 2007), this event is unlikely to have caused dramatic tectonic effects as far afield as Mongolia or Siberia. In these locations, the influence of the Mongol-Okhotsk orogeny is generally judged to be more significant (Jolivet et al., 2009), although the final closure of the Mongol-Okhotsk Ocean probably took place during the Early Cretaceous, rather than Late Cretaceous (Metelkin et al., 2010). Some authors have argued that ongoing tectonic forces associated with the Mongol-Okhotsk orogeny, such as orogenic collapse

and extension, continued to have an influence on Central Asia for an extended period following the actual collision (Fan et al., 2003; Graham et al., 2001; Jolivet et al., 2009, 2013).

5.2. Comparison With Neighboring Regions

The results presented in this study are generally in agreement with earlier work in the central Chinese Tianshan. Dumitru et al. (2001) and Jolivet et al. (2010) found that some mountain ranges experienced Late Triassic to Early Jurassic cooling followed by a period of apparent quiescence in the Middle Jurassic to Cretaceous. Initial formation of an extensive planation surface over most of Central Asia began during this period of relative stability (Jolivet et al., 2013). This planation surface is still preserved in various places throughout Central Asia (Allen et al., 2001; Jolivet et al., 2007, 2013; Vassallo et al., 2007).

The Late Cretaceous reactivation of the easternmost Tianshan bears many similarities to localized Late Cretaceous to early Paleogene deformation recorded in the South Borohoro and Narat Ranges of the central Chinese Tianshan (Jolivet et al., 2010). These areas possess similar basement architecture to the easternmost Tianshan and also experienced uplift associated with the reactivation of older shear zones. The steep, deeply incised northern slopes and tilted southern flank of the South Borohoro Range especially resembles the topography and geomorphology of the easternmost Tianshan (Jolivet et al., 2010). These regions all seem to have experienced similar, localized deformation focused around reactivated inherited structures in what was probably a transpressive tectonic setting (Jolivet et al., 2013). Sedimentological records from the northern Tarim Basin and the southern Junggar Basin show increased rates of basin subsidence during the Late Cretaceous and early Paleogene, accompanied by the deposition of coarse clastic sediments (Hendrix et al., 1992). Following the localized deformation and uplift described above, the area once again experienced erosion and planation, forming a new regional erosional surface in western Mongolia and the Chinese Tianshan (Cunningham et al., 2003; Devyatkin, 1974; Heilbronn et al., 2015).

Late Cenozoic cooling has also been reported from areas within the Chinese Tianshan, generally limited to areas near major faults. Several studies have reported Oligocene-Miocene ages from Bogda Shan (Shen et al., 2006, 2008), to the immediate east of Urumqi, and a wide range of Cenozoic ages from major faults in the ranges of the Tianshan to the west of the city (Dumitru et al., 2001; Hendrix et al., 1994; Jolivet et al., 2010; Lü et al., 2013; Wang, Li, et al., 2009). However, Cenozoic AFT ages were not found in this study, suggesting that in contrast to the ranges farther to the west, Cenozoic exhumation in the easternmost Tianshan was not extensive enough to expose rocks that record Cenozoic cooling.

The mountain ranges of the Kyrgyz Tianshan experienced a variety of Mesozoic thermal histories that span most of the Jurassic and Cretaceous. Periods of enhanced cooling have been identified at 230–190 Ma, 150–130 Ma, 110–90 Ma, and 75–65 Ma (De Grave et al., 2013; Glorie et al., 2011; Glorie & De Grave, 2016; Macaulay et al., 2014; Sobel, Oskin, et al., 2006). Since these ranges are located far to the west of the study region, it is difficult to link the varying histories of the Kyrgyz Tianshan to the easternmost Tianshan in a more precise manner. During the Cenozoic, many of the inherited Paleozoic structures of the Kyrgyz Tianshan were reactivated in response to the India-Eurasia collision and therefore record Oligocene-Pliocene AFT ages (Bande et al., 2017; De Grave et al., 2013; Glorie et al., 2011; Macaulay et al., 2014; Sobel, Oskin, et al., 2006).

Work in the Siberian Altai, to the north of the Tianshan, found a phase of rapid cooling during the Late Triassic to early Jurassic that was attributed to the initiation of the Mongol-Okhotsk orogeny (Glorie et al., 2012; Metelkin et al., 2007). This cooling signal is coeval with cooling in the south of the CAOB, where it is more commonly associated with the Qiangtang collision based on geographical proximity (Glorie & De Grave, 2016; Schwab et al., 2004; Zhai et al., 2011). The Siberian Altai furthermore records slower cooling from the Late Jurassic to Early Cretaceous as a result of slow regional denudation at that time, which was followed by a phase of more rapid cooling during the Late Cretaceous and the early Paleogene. The latter rapid cooling phase was interpreted to be the result of the collapse of the Mongol-Okhotsk orogeny and the subsequent transition into the Lake Baikal rifting regime with block reorganization in the eastern CAOB (Jolivet et al., 2009). The Chinese Altai similarly records a Late Cretaceous cooling phase, albeit with an earlier cessation of cooling that was interpreted to have ended prior to the end of the Mesozoic (Yuan et al., 2006).

In contrast to the thermal histories proposed for the Siberian and Chinese Altai, work in the Gobi Altai has uncovered little evidence for a Late Cretaceous phase of cooling (Jolivet et al., 2007; Vassallo et al., 2007). The Gobi Altai appears to have experienced Early to Middle Jurassic cooling followed by an extended period of thermal quiescence prior to very recent reactivation in response to the India-Eurasia collision.

To the immediate southeast of the easternmost Tianshan, the Beishan plateau records evidence for Late Triassic to early Jurassic cooling and a later Cretaceous phase of cooling, suggesting that both regions experienced a comparable thermotectonic history during the Mesozoic (Gillespie et al., 2017; Tian et al., 2016). As in the easternmost Tianshan, no thermochronological evidence was found within the thermal history record of the Beishan to suggest any Cenozoic activity. The Beishan differs from the mountains to the north in that it has very subdued internal topography and presents no structural or topographic evidence for significant late Cenozoic reactivation (Cunningham et al., 2003).

5.3. Comparison With Existing Data in the Easternmost Tianshan

Previous AFT work in the easternmost Tianshan found much younger ages than the results of this study. All the central ages for the easternmost Tianshan presented in Wang et al. (2008) were less than 33 Ma in age, with Miocene ages dominating the region. This result is highly unusual for the Tianshan, where Cretaceous and Jurassic ages are most prevalent regionally (Figure 1), while younger ages are typically concentrated in reactivated sutures and other major inherited structures (e.g., Glorie et al., 2011). Miocene ages all throughout the easternmost Tianshan would imply that the area has undergone regional exhumation to an equivalent degree as in the Kyrgyz Tianshan or the Pamir. The presence of low-altitude planation surfaces already raises questions about the conclusions of Wang et al. (2008) as they constrain the amount of uplift that could have occurred during the Cenozoic (Cunningham et al., 2003).

Wang et al. (2008) describes the sample preparation and analytical procedure in sufficient detail that a possible explanation for the discrepancy can be found. Apatite mounts were submerged in a $HN0_3$ concentration of 7% (presumably vol %) at 20°C for 35 s during the spontaneous fission track etching procedure. While these parameters are within the variation in preparation technique used by different laboratories around the world, experiments presented in Seward et al. (2000) found that these etching conditions resulted in the majority of tracks being underetched. Seward et al. (2000) recommended that a further 20 s of etching at these conditions (i.e., 55 s total) was required for complete etching to occur and for the results to be comparable with the conditions they found to be optimal—that is, at 21°C for 20 s in 5 *M* HNO_3. The number of spontaneous tracks counted for each sample is also very low (mostly <200, 50% of samples $\ll 100$).

Consequently, the unusual distribution of young central ages may be a result of this experimental factor. The lack of GPS coordinates or detailed small-scale maps makes the exact locations of the samples from this study difficult to precisely ascertain, but it appears as though several do overlap closely with samples from this study. Several were seemingly taken along the mountain pass where both BH17 and BH19 were obtained (Figure 1). The Cretaceous central ages of these two samples contrast strongly with the Oligocene-Miocene central ages presented in Wang et al. (2008).

6. Conclusions

The easternmost Tianshan experienced three phases of cooling throughout the Mesozoic and Cenozoic, only two of which this study has directly revealed via thermochronological evidence. An initial phase of cooling during the early to middle Triassic was driven by regional exhumation in response to the final closure of the Paleoasian Ocean, with the collision of the Tarim Craton to the immediate south of the modern Tianshan. An extended period of slow cooling lasting until the Late Cretaceous was followed by a phase of enhanced cooling at ~80 Ma. Cooling at this time was limited to the area within the bounding faults of the modern mountain range. The thermal structure established during Late Cretaceous cooling was preserved in the stable upper few kilometers of the crust until late Cenozoic reactivation, when the ranges were variably uplifted and exhumed, creating the distribution of ages that we see today. Late Cenozoic reactivation of the easternmost Tianshan is evident from structural relationships and

topographic analysis but cannot be constrained by thermochronological data due to the low level of exhumation. The combination of AFT, AHe, and structural/topographic data synthesized here is incompatible with the conclusions of Wang et al. (2008).

Acknowledgments
This work was financially supported by the 973 Program (2014CB440801), the National Natural Science Foundation of China (grants 41230207 and 41302167), the Australian Research Council Discovery Project (DP150101730), and the IGCP project 592. A. S. C. is funded by an Australian Research Council Future Fellowship (FT120100340). J. G. is supported by an Australian Government Research Training Program Scholarship. M. D. is supported by the AuScope NCRIS2 program, Australian Scientific Instruments Pty Ltd., and Australian Research Council Discovery funding scheme (DP160102427). M. D. thanks I. Dunkl for sharing PepiFLEX software for ICP-MS data reduction and C. May and C. Scadding (TSW Analytical) for help with the solution ICP-MS analyses. Adelaide Microscopy and Benjamin Wade are thanked for their assistance with the use of the LA-ICP-MS. Data and figures supporting the conclusions presented here can be found in the supporting information. We thank G. Heilbronn and an anonymous reviewer for their constructive and helpful feedback on the initial manuscript. This paper forms TRaX record 372.

References

Allen, M. B., Alsop, A. I., & Zhemchuzhnikov, V. G. (2001). Dome and basin refolding and transpressive inversion along the Karatau Fault System, southern Kazakhstan. *Journal of the Geological Society*, *158*(1), 83–95.

Allen, M. B., Anderson, L., Searle, R. C., & Buslov, M. (2006). Oblique rift geometry of the West Siberian Basin: Tectonic setting for the Siberian flood basalts. *Journal of the Geological Society*, *163*(6), 901–904.

Avouac, J. P., Tapponnier, P., Bai, M., You, H., & Wang, G. (1993). Active thrusting and folding along the northern Tien Shan and Late Cenozoic rotation of the Tarim relative to Dzungaria and Kazakhstan. *Journal of Geophysical Research*, *98*(B4), 6755–6804.

Bande, A., Sobel, E. R., Mikolaichuk, A., Schmidt, A., & Stockli, D. F. (2017). Exhumation history of the western Kyrgyz Tien Shan: Implications for intramontane basin formation. *Tectonics*, *36*, 163–180. https://doi.org/10.1002/2016TC004284

Barbarand, J., Carter, A., Wood, I., & Hurford, T. (2003). Compositional and structural control of fission-track annealing in apatite. *Chemical Geology*, *198*(1–2), 107–137.

Biske, Y. S., & Seltmann, R. (2010). Paleozoic Tian-Shan as a transitional region between the Rheic and Urals-Turkestan oceans. *Gondwana Research*, *17*(2), 602–613.

Brown, R. W., Beucher, R., Roper, S., Persano, C., Stuart, F., & Fitzgerald, P. (2013). Natural age dispersion arising from the analysis of broken crystals. Part I: Theoretical basis and implications for the apatite (U–Th)/He thermochronometer. *Geochimica et Cosmochimica Acta*, *122*, 478–497.

Carpena, J., & Lacout, J.-L. (2010). Thermal annealing of fission tracks in synthetic apatites. *Nuclear Instruments and Methods in Physics Research Section B: Beam Interactions with Materials and Atoms*, *268*(19), 3191–3194.

Carpena, J., Kienast, J.-R., Ouzegane, K., & Jehanno, C. (1988). Evidence of the contrasted fission-track clock behavior of the apatites from In Ouzzal carbonatites (northwest Hoggar): The low-temperature thermal history of an Archean basement. *Geological Society of America Bulletin*, *100*(8), 1237–1243.

Charvet, J., Shu, L., Laurent-Charvet, S., Wang, B., Faure, M., Cluzel, D., … De Jong, K. (2011). Palaeozoic tectonic evolution of the Tianshan belt, NW China. *Science China Earth Sciences*, *54*(2), 166–184.

Cunningham, D. (2013). Mountain building processes in intracontinental oblique deformation belts: Lessons from the Gobi Corridor, Central Asia. *Journal of Structural Geology*, *46*(0), 255–282.

Cunningham, D., Owen, L., Snee, L., & Li, J. (2003). Structural framework of a major intracontinental orogenic termination zone: The easternmost Tien Shan, China. *Journal of the Geological Society*, *160*, 575–590.

Danišík, M., Kuhlemann, J., Dunkl, I., Evans, N. J., Székely, B., & Frisch, W. (2012). Survival of ancient landforms in a collisional setting as revealed by combined fission track and (U-Th)/He thermochronometry: A case study from Corsica (France). *The Journal of Geology*, *120*(2), 155–173.

Danišík, M., Štěpančíková, P., & Evans, N. J. (2012). Constraining long-term denudation and faulting history in intraplate regions by multisystem thermochronology: An example of the Sudetic Marginal Fault (Bohemian Massif, central Europe). *Tectonics*, *31*, TC2003. https://doi.org/10.1029/2011TC003012

De Grave, J., Buslov, M. M., & Van den Haute, P. (2007). Distant effects of India–Eurasia convergence and Mesozoic intracontinental deformation in Central Asia: Constraints from apatite fission-track thermochronology. *Journal of Asian Earth Sciences*, *29*(2–3), 188–204.

De Grave, J., Glorie, S., Buslov, M. M., Stockli, D. F., McWilliams, M. O., Batalev, V. Y., & Van den Haute, P. (2013). Thermo-tectonic history of the Issyk-Kul basement (Kyrgyz Northern Tien Shan, Central Asia). *Gondwana Research*, *23*(3), 998–1020.

Devyatkin, E. (1974). Structures and formational complexes of the Cenozoic activated stage. *Tectonics of the Mongolian People's Republic: Moscow, Nauka*, *41*, 182–195.

Donelick, R. A., Ketcham, R. A., & Carlson, W. D. (1999). Variability of apatite fission-track annealing kinetics: II. Crystallographic orientation effects. *American Mineralogist*, *84*(9), 1224–1234.

Dumitru, T. A., Zhou, D., Chang, E. Z., Graham, S. A., Hendrix, M. S., Sobel, E. R., & Carroll, A. R. (2001). Uplift, exhumation, and deformation in the Chinese Tian Shan. *Geological Society of America Memoirs*, *194*, 71–99.

Ehlers, T. A., & Farley, K. A. (2003). Apatite (U–Th)/He thermochronometry: Methods and applications to problems in tectonic and surface processes. *Earth and Planetary Science Letters*, *206*(1–2), 1–14.

Evans, N. J., Byrne, J. P., Keegan, J. T., & Dotter, L. E. (2005). Determination of uranium and thorium in zircon, apatite, and fluorite: Application to laser (U-Th)/He thermochronology. *Journal of Analytical Chemistry*, *60*(12), 1159–1165.

Fan, W.-M., Guo, F., Wang, Y.-J., & Lin, G. (2003). Late Mesozoic calc-alkaline volcanism of post-orogenic extension in the northern Da Hinggan Mountains, northeastern China. *Journal of Volcanology and Geothermal Research*, *121*(1–2), 115–135.

Farley, K. A. (2002). (U-Th)/He dating: Techniques, calibrations, and applications. *Reviews in Mineralogy and Geochemistry*, *47*(1), 819–844.

Farley, K. A., Wolf, R. A., & Silver, L. T. (1996). The effects of long alpha-stopping distances on (U-Th)/He ages. *Geochimica et Cosmochimica Acta*, *60*(21), 4223–4229.

Fitzgerald, P. G., Baldwin, S. L., Webb, L. E., & O'Sullivan, P. B. (2006). Interpretation of (U–Th)/He single grain ages from slowly cooled crustal terranes: A case study from the Transantarctic Mountains of southern Victoria Land. *Chemical Geology*, *225*(1–2), 91–120.

Galbraith, R. F. (1990). The radial plot: Graphical assessment of spread in ages. *International Journal of Radiation Applications and Instrumentation. Part D. Nuclear Tracks and Radiation Measurements*, *17*(3), 207–214.

Gallagher, K. (2012). Transdimensional inverse thermal history modeling for quantitative thermochronology. *Journal of Geophysical Research*, *117*, B04208. https://doi.org/10.1029/2011JB008825

Gautheron, C., Tassan-Got, L., Barbarand, J., & Pagel, M. (2009). Effect of alpha-damage annealing on apatite (U–Th)/He thermochronology. *Chemical Geology*, *266*(3–4), 157–170.

Gillespie, J., Glorie, S., Xiao, W., Zhang, Z., Collins, A. S., Evans, N., … De Grave, J. (2017). Mesozoic reactivation of the Beishan, southern Central Asian Orogenic Belt: Insights from low-temperature thermochronology. *Gondwana Research*, *43*, 107–122.

Gleadow, A. J. W., Duddy, I. R., Green, P. F., & Lovering, J. F. (1986). Confined fission track lengths in apatite: A diagnostic tool for thermal history analysis. *Contributions to Mineralogy and Petrology*, *94*(4), 405–415.

Gleadow, A. J. W., Gleadow, S. J., Belton, D. X., Kohn, B. P., Krochmal, M. S., & Brown, R. W. (2009). Coincidence mapping—A key strategy for the automatic counting of fission tracks in natural minerals. *Geological Society, London, Special Publications*, *324*(1), 25–36.
Glorie, S., Alexandrov, I., Nixon, A., Jepson, G., Gillespie, J., & Jahn, B.-M. (2017). Thermal and exhumation history of Sakhalin Island (Russia) constrained by apatite U-Pb and fission track thermochronology. *Journal of Asian Earth Sciences*, *143*, 326–342.
Glorie, S., & De Grave, J. (2016). Exhuming the Meso-Cenozoic Kyrgyz Tianshan and the Siberian Altai-Sayan: A review based on low-temperature thermochronology. *Geoscience Frontiers*, *7*(2), 155–170.
Glorie, S., De Grave, J., Buslov, M. M., Zhimulev, F. I., Elburg, M. A., & Van den Haute, P. (2012). Structural control on Meso-Cenozoic tectonic reactivation and denudation in the Siberian Altai: Insights from multi-method thermochronometry. *Tectonophysics*, *544–545*(0), 75–92.
Glorie, S., De Grave, J., Buslov, M. M., Zhimulev, F. I., Stockli, D. F., Batalev, V. Y., … Elburg, M. A. (2011). Tectonic history of the Kyrgyz South Tien Shan (Atbashi-Inylchek) suture zone: The role of inherited structures during deformation-propagation. *Tectonics*, *30*, TC6016. https://doi.org/10.1029/2011TC002949
Graham, S. A., Hendrix, M. S., Johnson, C. L., Badamgarav, D., Badarch, G., Amory, J., … Hacker, B. R. (2001). Sedimentary record and tectonic implications of Mesozoic rifting in southeast Mongolia. *Geological Society of America Bulletin*, *113*(12), 1560–1579.
Green, P. F., Duddy, I. R., Gleadow, A. J. W., Tingate, P. R., & Laslett, G. M. (1986). Thermal annealing of fission tracks in apatite: 1. A qualitative description. *Chemical Geology: Isotope Geoscience*, *59*(0), 237–253.
Hasebe, N., Barbarand, J., Jarvis, K., Carter, A., & Hurford, A. J. (2004). Apatite fission-track chronometry using laser ablation ICP-MS. *Chemical Geology*, *207*(3–4), 135–145.
Heilbronn, G., Boulvais, P., Marchand, E., Robin, C., Bourquin, S., Barrier, L., … Jolivet, M. (2015). Stable isotope characterization of pedogenic and lacustrine carbonates from the Chinese Tian Shan: Constraints on the Mesozoic–Lower Cenozoic palaeoenvironmental evolution. *Chemie der Erde - Geochemistry*, *75*(1), 133–141.
Hendriks, B. W. H., & Redfield, T. F. (2005). Apatite fission track and (U-Th)/He data from Fennoscandia: An example of underestimation of fission track annealing in apatite. *Earth and Planetary Science Letters*, *236*(1–2), 443–458.
Hendrix, M. S. (2000). Evolution of Mesozoic sandstone compositions, Southern Junggar, Northern Tarim, and Western Turpan Basins, Northwest China: A detrital record of the ancestral Tian Shan. *Journal of Sedimentary Research*, *70*(3), 520–532.
Hendrix, M. S., Dumitru, T. A., & Graham, S. A. (1994). Late Oligocene-early Miocene unroofing in the Chinese Tian Shan: An early effect of the India-Asia collision. *Geology*, *22*(6), 487–490.
Hendrix, M. S., Graham, S. A., Carroll, A. R., Sobel, E. R., McKnight, C. L., Schulein, B. J., & Wang, Z. (1992). Sedimentary record and climatic implications of recurrent deformation in the Tian Shan: Evidence from Mesozoic strata of the north Tarim, south Junggar, and Turpan basins, northwest China. *GSA Bulletin*, *104*(1), 53–79.
Jolivet, M., De Boisgrollier, T., Petit, C., Fournier, M., Sankov, V. A., Ringenbach, J. C., … Anisimova, S. V. (2009). How old is the Baikal Rift Zone? Insight from apatite fission track thermochronology. *Tectonics*, *28*, TC3008. https://doi.org/10.1029/2008TC002404
Jolivet, M., Dominguez, S., Charreau, J., Chen, Y., Li, Y., & Wang, Q. (2010). Mesozoic and Cenozoic tectonic history of the central Chinese Tian Shan: Reactivated tectonic structures and active deformation. *Tectonics*, *29*, TC6019. https://doi.org/10.1029/2010TC002712
Jolivet, M., Heilbronn, G., Robin, C., Barrier, L., Bourquin, S., Guo, Z., … Fu, B. (2013). Reconstructing the Late Palaeozoic-Mesozoic topographic evolution of the Chinese Tian Shan: Available data and remaining uncertainties. *Advances in Geosciences*, *37*, 7–18.
Jolivet, M., Ritz, J.-F., Vassallo, R., Larroque, C., Braucher, R., Todbileg, M., … Arzhanikov, S. (2007). Mongolian summits: An uplifted, flat, old but still preserved erosion surface. *Geology*, *35*(10), 871–874.
Käßner, A., Ratschbacher, L., Jonckheere, R., Enkelmann, E., Khan, J., Sonntag, B.-L., … Oimahmadov, I. (2016). Cenozoic intracontinental deformation and exhumation at the northwestern tip of the India-Asia collision—southwestern Tian Shan, Tajikistan, and Kyrgyzstan. *Tectonics*, *35*, 2171–2194. https://doi.org/10.1002/2015TC003897
Ketcham, R. A., Carter, A., Donelick, R. A., Barbarand, J., & Hurford, A. J. (2007). Improved modeling of fission-track annealing in apatite. *American Mineralogist*, *92*(5–6), 799–810.
Ketcham, R. A., Donelick, R. A., & Carlson, W. D. (1999). Variability of apatite fission-track annealing kinetics: III. Extrapolation to geological time scales. *American Mineralogist*, *84*(9), 1235–1255.
Laurent-Charvet, S., Charvet, J., Monié, P., & Shu, L. (2003). Late Paleozoic strike-slip shear zones in eastern central Asia (NW China): New structural and geochronological data. *Tectonics*, *22*(2), 1009. https://doi.org/10.1029/2001TC901047
Lehmann, J., Schulmann, K., Lexa, O., Corsini, M., Kröner, A., Štípská, P., … Otgonbator, D. (2010). Structural constraints on the evolution of the Central Asian Orogenic Belt in SW Mongolia. *American Journal of Science*, *310*(7), 575–628.
Lü, H., Chang, Y., Wang, W., & Zhou, Z. (2013). Rapid exhumation of the Tianshan Mountains since the early Miocene: Evidence from combined apatite fission track and (U-Th)/He thermochronology. *Science China Earth Sciences*, *56*(12), 2116–2125.
Ma, X., Shu, L., & Meert, J. G. (2015). Early Permian slab breakoff in the Chinese Tianshan belt inferred from the post-collisional granitoids. *Gondwana Research*, *27*(1), 228–243.
Ma, Q., Shu, L., & Zhu, W. (2006). Mesozoic-Cenozoic burial, uplift and exhumation: A profile along the Urumqi-Korla highway in the Tianshan Mountains. *Xinjiang Geology*, *24*(2), 99–104.
Macaulay, E. A., Sobel, E. R., Mikolaichuk, A., Kohn, B., & Stuart, F. M. (2014). Cenozoic deformation and exhumation history of the Central Kyrgyz Tien Shan. *Tectonics*, *33*, 135–165. https://doi.org/10.1002/2013TC003376
Macaulay, E. A., Sobel, E. R., Mikolaichuk, A., Landgraf, A., Kohn, B., & Stuart, F. (2013). Thermochronologic insight into late Cenozoic deformation in the basement-cored Terskey Range, Kyrgyz Tien Shan. *Tectonics*, *32*, 487–500. https://doi.org/10.1002/tect.20040
McDowell, F. W., McIntosh, W. C., & Farley, K. A. (2005). A precise 40Ar–39Ar reference age for the Durango apatite (U–Th)/He and fission-track dating standard. *Chemical Geology*, *214*(3–4), 249–263.
Metelkin, D. V., Gordienko, I. V., & Klimuk, V. S. (2007). Paleomagnetism of Upper Jurassic basalts from Transbaikalia: New data on the time of closure of the Mongol-Okhotsk Ocean and Mesozoic intraplate tectonics of Central Asia. *Russian Geology and Geophysics*, *48*(10), 825–834.
Metelkin, D. V., Vernikovsky, V. A., Kazansky, A. Y., & Wingate, M. T. D. (2010). Late Mesozoic tectonics of Central Asia based on paleomagnetic evidence. *Gondwana Research*, *18*(2–3), 400–419.
Molnar, P., & Tapponnier, P. (1975). Cenozoic tectonics of Asia: Effects of a continental collision: Features of recent continental tectonics in Asia can be interpreted as results of the India-Eurasia collision. *Science*, *189*(4201), 419–426.
O'Sullivan, P. B., & Parrish, R. R. (1995). The importance of apatite composition and single-grain ages when interpreting fission track data from plutonic rocks: A case study from the Coast Ranges, British Columbia. *Earth and Planetary Science Letters*, *132*(1), 213–224.
Schwab, M., Ratschbacher, L., Siebel, W., McWilliams, M., Minaev, V., Lutkov, V., … Wooden, J. L. (2004). Assembly of the Pamirs: Age and origin of magmatic belts from the southern Tien Shan to the southern Pamirs and their relation to Tibet. *Tectonics*, *23*, TC4002. https://doi.org/10.1029/2003TC001583

Seward, D., Spikings, R., Viola, G., Kounov, A., Ruiz, G., & Naeser, N. (2000). Etch times and operator variation for spontaneous track length measurements in apatites: An intra-laboratory check. *On Track*, *10*(2), 19–21.

Shen, C., Mei, L., Peng, L., Zhang, S., Liu, L., & Tang, J. (2006). Fission track evidence for the Mesozoic-Cenozoic tectonic uplift of Mt. Bogda, Xinjiang, northwest China. *Chinese Journal of Geochemistry*, *25*(2), 143.

Shen, C., Mei, L., Zhang, S., Liu, L., Tang, J., Zhou, F., … Luo, J. (2008). Fission-track dating evidence on space-time difference of Mesozoic-Cenozoic uplift of the Yilianhabierga Mountain Bogeda Mountain. *Journal of Mineralogy and Petrology*, *28*(2), 63–70.

Sobel, E. R., Chen, J., & Heermance, R. V. (2006). Late Oligocene–Early Miocene initiation of shortening in the Southwestern Chinese Tian Shan: Implications for Neogene shortening rate variations. *Earth and Planetary Science Letters*, *247*(1–2), 70–81.

Sobel, E. R., & Dumitru, T. A. (1997). Thrusting and exhumation around the margins of the western Tarim basin during the India-Asia collision. *Journal of Geophysical Research*, *102*(B3), 5043–5063. https://doi.org/10.1029/96JB03267

Sobel, E. R., Oskin, M., Burbank, D., & Mikolaichuk, A. (2006). Exhumation of basement-cored uplifts: Example of the Kyrgyz Range quantified with apatite fission track thermochronology. *Tectonics*, *25*, TC2008. https://doi.org/10.1029/2005TC001809

Tang, W., Zhang, Z., Li, J., Li, K., Luo, Z., & Chen, Y. (2015). Mesozoic and Cenozoic uplift and exhumation of the Bogda Mountain, NW China: Evidence from apatite fission track analysis. *Geoscience Frontiers*, *6*(4), 617–625.

Tian, Z., Xiao, W., Zhang, Z., & Lin, X. (2016). Fisson-track constrains on superposed folding in the Beishan orogenic belt, southernmost Altaids. *Geoscience Frontiers*, *7*(2), 181–196.

Vassallo, R., Jolivet, M., Ritz, J. F., Braucher, R., Larroque, C., Sue, C., … Javkhlanbold, D. (2007). Uplift age and rates of the Gurvan Bogd system (Gobi-Altay) by apatite fission track analysis. *Earth and Planetary Science Letters*, *259*(3–4), 333–346.

Vermeesch, P. (2009). RadialPlotter: A Java application for fission track, luminescence and other radial plots. *Radiation Measurements*, *44*(4), 409–410.

Vermeesch, P. (2017). Statistics for LA-ICP-MS based fission track dating. *Chemical Geology*, *456*, 19–27.

Wang, C., Gu, L., Zhang, Z., Wu, C., Tang, J., & Tang, X. (2009). Petrogenesis and geological implications of the Permian high-K calc-alkaline granites in Harlik Mountains of eastern Tianshan, NW China. *Acta Petrologica Sinica*, *25*(6), 1499–1511.

Wang, Q., Li, S., & Du, Z. (2009). Differential uplift of the Chinese Tianshan since the Cretaceous: Constraints from sedimentary petrography and apatite fission-track dating. *International Journal of Earth Sciences (Geologische Rundschau)*, *98*(6), 1341–1363.

Wang, Z., Li, T., Zhang, J., Liu, Y., & Ma, Z. (2008). The uplifting process of the Bogda Mountain during the Cenozoic and its tectonic implication. *Science in China Series D: Earth Sciences*, *51*(4), 579–593.

Windley, B. F., Alexeiev, D., Xiao, W., Kröner, A., & Badarch, G. (2007). Tectonic models for accretion of the Central Asian Orogenic Belt. *Journal of the Geological Society*, *164*(1), 31–47.

Windley, B. F., Allen, M. B., Zhang, C., Zhao, Z. Y., & Wang, G. R. (1990). Paleozoic accretion and Cenozoic redeformation of the Chinese Tien Shan Range, Central Asia. *Geology*, *18*(2), 128–131.

Wolf, R. A., Farley, K. A., & Kass, D. M. (1998). Modeling of the temperature sensitivity of the apatite (U–Th)/He thermochronometer. *Chemical Geology*, *148*(1–2), 105–114.

Xiao, W., Windley, B., Huang, B., Han, C., Yuan, C., Chen, H., … Li, J. (2009). End-Permian to mid-Triassic termination of the accretionary processes of the southern Altaids: Implications for the geodynamic evolution, Phanerozoic continental growth, and metallogeny of Central Asia. *The International Journal of Earth Sciences (Geologische Rundschau)*, *98*(6), 1189–1217.

Xiao, W., Windley, B. F., Allen, M. B., & Han, C. (2013). Paleozoic multiple accretionary and collisional tectonics of the Chinese Tianshan orogenic collage. *Gondwana Research*, *23*(4), 1316–1341.

Xiao, W., Zhang, L., Qin, K., Sun, S., & Li, J. (2004). Paleozoic accretionary and collisional tectonics of the eastern Tianshan (China): Implications for the continental growth of central Asia. *American Journal of Science*, *304*(4), 370–395.

Yuan, W., Carter, A., Dong, J., Bao, Z., An, Y., & Guo, Z. (2006). Mesozoic–Tertiary exhumation history of the Altai Mountains, northern Xinjiang, China: New constraints from apatite fission track data. *Tectonophysics*, *412*(3–4), 183–193.

Yuan, C., Sun, M., Wilde, S., Xiao, W., Xu, Y., Long, X., & Zhao, G. (2010). Post-collisional plutons in the Balikun area, East Chinese Tianshan: Evolving magmatism in response to extension and slab break-off. *Lithos*, *119*(3–4), 269–288.

Zhai, Q.-G., Jahn, B.-M., Zhang, R.-Y., Wang, J., & Su, L. (2011). Triassic Subduction of the Paleo-Tethys in northern Tibet, China: Evidence from the geochemical and isotopic characteristics of eclogites and blueschists of the Qiangtang Block. *Journal of Asian Earth Sciences*, *42*(6), 1356–1370.

Zhang, Z., Zhu, W., Shu, L., Wan, J., Yang, W., Su, J., & Zheng, B. (2009). Apatite fission track thermochronology of the Precambrian Aksu blueschist, NW China: Implications for thermo–tectonic evolution of the north Tarim basement. *Gondwana Research*, *16*(2), 182–188.